



Global Modeling and Assimilation Office

GMAO Office Note No. 23 (Version 1.0)

The Implementation of GOCART-2G in GEOS Forward Processing

Release Date: 02/04/2026

**Global Modeling and Assimilation Office
Earth Sciences Division
NASA Goddard Space Flight Center
Greenbelt, Maryland 20771**

This page intentionally left blank.

The Implementation of GOCART Second Generation in GEOS Forward Processing

Document maintained by Allison Collow (GMAO, UMBC)

This document should be cited as
Collow, A., Buchard, V., Castellanos, P., Lucchesi, R., and da Silva, A., 2026: The
Implementation of GOCART Second Generation in GEOS Forward Processing. GMAO Office
Note No. 23 (Version 1.0), 23 pp, available from http://gmao.gsfc.nasa.gov/pubs/office_notes.

Approved by:

Steven Pawson Date
Chief, Global Modeling and Assimilation Office
Code 610.1, NASA GSFC

REVISION HISTORY

Version Number	Revision Date	Extent of Changes
1.0	02/04/2026	Baseline

1. Introduction	1
2. File Specification Changes	1
3. Guidance on the use of PM_{2.5}	4
4. Science Impacts of GOCART-2G	5
4.1 Emissions	6
4.2 Total Aerosol Optical Depth	7
4.3 Organic, Brown, and Black Carbon	10
4.4 Sulfate	13
4.5 Nitrate	15
4.6 Sea Salt	17
4.7 Dust.....	19
Summary	21
Acknowledgements	21
References	21

Table of Contents

1. Introduction

Version 5.43.0 of the GEOS Forward Processing (FP) system marks the introduction of GOCART Second Generation (GOCART-2G) as the underlying aerosol module within GEOS. In this upgrade, the source code governing aerosols was refactored to improve flexibility and efficiency, which was necessary to enable future development. These code changes were bundled with science updates to comprise GOCART-2G as detailed in Collow et al. (2024). From a scientific perspective, the largest changes impact the carbonaceous aerosol. Organic aerosol was split into components from anthropogenic sources (still termed organic carbon) and biomass burning sources (referred to as brown carbon). This allows for differing treatments of the radiative absorption properties of organic and brown carbon. Furthermore, secondary organic aerosol was added as a tracer and is used to produce organic and brown carbon from volatile organic compound (VOC) emissions. While the intention was to make other species including dust, sea salt, sulfate and nitrate identical before and after the code changes, there are slight differences due to bug fixes in the code. These changes in the aerosol modeling have been adopted along with a more recent dataset for prescribing anthropogenic emissions. Aerosol size bins and optical properties have not changed other than the inclusion of a new set of optical properties for brown carbon which are detailed in Collow et al. (2023). [LINK: <https://gmao.gsfc.nasa.gov/pubs/docs/Collow1489.pdf>.]

With the introduction of new tracers and modifications to the code, the variables within the aerosol file collections have changed. This is further described in Section 2, and guidance pertaining to a new diagnostic variable, PM25 or particulate matter with a geometric diameter smaller than 2.5 microns, can be found in Section 3. Section 4 provides a detailed evaluation of anthropogenic emissions and aerosol optical depth (AOD) in the new system against existing GEOS products.

2. File Specification Changes

While the GEOS-FP aerosol file collection names remain unchanged, additional variables are added (Table 1), changes are made to variable short and long names to improve usability (Table 2), and obsolete fields (DUAERIDX and SSAERIDX) are removed. There are three categories of fields that have been added: 1) those necessary for the aerosol lifecycle of brown carbon; 2) aerosol extinction and scattering within the stratosphere; and 3) surface particulate matter. Stratospheric aerosol optical thickness is calculated by computing the aerosol extinction from the tropopause height using the blended estimate, TROPPE, to the top of the atmosphere. Additional guidance pertaining to surface particulate matter can be found in Section 3.

Table 1. List of new aerosol fields in GEOS 5.43.0

Variable Name	Description	File Collection
BRPHILIC	Hydrophilic brown carbon aerosol mixing ratio	inst3_3d_aer_Nv
BRPHOBIC	Hydrophobic brown carbon aerosol mixing ratio	inst3_3d_aer_Nv
H	Mid-layer heights	inst3_3d_aer_Nv
BREMAN	Anthropogenic emissions of brown carbon	tavg3_2d_adg_Nx

BREMBB	Biomass burning emissions of brown carbon	tavg3_2d_adg_Nx
BREMBF	Biofuel emissions of brown carbon	tavg3_2d_adg_Nx
BRPHOBICDP	Dry deposition of hydrophobic brown carbon	tavg3_2d_adg_Nx
BRPHOBICEM	Emissions of hydrophobic brown carbon	tavg3_2d_adg_Nx
BRPHOBICWT	Wet deposition of hydrophobic brown carbon	tavg3_2d_adg_Nx
BRPHILICDP	Dry deposition of hydrophilic brown carbon	tavg3_2d_adg_Nx
BRPHILICEM	Emissions of hydrophilic brown carbon	tavg3_2d_adg_Nx
BRPHILICWT	Wet deposition of hydrophilic brown carbon	tavg3_2d_adg_Nx
BRPSOA	Production of brown carbon from secondary organic aerosol	tavg3_2d_adg_Nx
BRSV	Convective scavenging of brown carbon	tavg3_2d_adg_Nx
BCSTEXTTAU	Black Carbon Stratospheric Aerosol Optical Thickness at 550 nm	tavg3_2d_aer_Nx
BCSTSCATAU	Black Carbon Stratospheric Aerosol Optical Thickness at 550 nm Due to Scattering	tavg3_2d_aer_Nx
BRANGSTR	Brown Carbon Aerosol Angstrom parameter [470-870 nm]	tavg3_2d_aer_Nx
BRCMASS	Brown Carbon Aerosol Column Mass Density	tavg3_2d_aer_Nx
BREXTTAU	Brown carbon aerosol optical depth at 550 nm	tavg3_2d_aer_Nx
BRSCATAU	Brown carbon aerosol optical depth at 550 nm due to scattering	tavg3_2d_aer_Nx
BRSMASS	Brown carbon aerosol surface mass concentration	tavg3_2d_aer_Nx
BRSTEXTTAU	Brown Carbon Stratospheric Aerosol Optical Thickness at 550 nm	tavg3_2d_aer_Nx
BRSTSCATAU	Brown Carbon Stratospheric Aerosol Optical Thickness at 550 nm Due to Scattering	tavg3_2d_aer_Nx
DUSTEXTTAU	Dust Stratospheric Aerosol Optical Thickness at 550 nm	tavg3_2d_aer_Nx
DUSTSCATAU	Dust Stratospheric Aerosol Optical Thickness at 550 nm Due to Scattering	tavg3_2d_aer_Nx
OCPSOA	Organic Aerosol SOA Production	tavg3_2d_adg_Nx
OCSTEXTTAU	Organic Carbon Stratospheric Aerosol Optical Thickness at 550 nm	tavg3_2d_aer_Nx
OCSTSCATAU	Organic Carbon Stratospheric Aerosol Optical Thickness at 550 nm Due to Scattering	tavg3_2d_aer_Nx
PM	Total Reconstructed Dry Particulate Matter	tavg3_2d_aer_Nx
PM25	Total Reconstructed Dry Particulate Matter smaller than 2.5 microns	tavg3_2d_aer_Nx
SSSTEXTTAU	Sea Salt Stratospheric Aerosol Optical Thickness at 550 nm	tavg3_2d_aer_Nx

SSSTSCATAU	Sea Salt Stratospheric Aerosol Optical Depth at 550 nm Due to Scattering	tavg3_2d_aer_Nx
SUSTEXTTAU	Sulfate Stratospheric Aerosol Optical Thickness at 550 nm	tavg3_2d_aer_Nx
SUSTSCATAU	Sulfate Stratospheric Aerosol Optical Depth at 550 nm Due to Scattering	tavg3_2d_aer_Nx
TOTSTEXTTAU	Total Stratospheric Aerosol Optical Thickness at 550 nm	tavg3_2d_aer_Nx
TOTSTSCATAU	Total Stratospheric Aerosol Optical Thickness at 550 nm Due to Scattering	tavg3_2d_aer_Nx

Table 2. List of aerosol fields with modified variable names in GEOS 5.43.0.

Variable in GEOS 5.29.4	Variable in GEOS 5.43.0	Variable Long Name	File Collection
NO3an1	NI001	Nitrate size bin 001 (fine mode nitrate)	inst3_3d_aer_Nv
NO3an2	NI002	Nitrate size bin 002	inst3_3d_aer_Nv
NO3an3	NI003	Nitrate size bin 003	inst3_3d_aer_Nv
BCDP001	BCPHOBICDP	Dry deposition of hydrophobic carbon	tavg3_2d_adg_Nx
BCDP002	BCPHILICDP	Dry deposition of hydrophilic carbon	tavg3_2d_adg_Nx
BCEM001	BCPHOBICEM	Emissions of hydrophobic black carbon	tavg3_2d_adg_Nx
BCEM002	BCPHILICEM	Emissions of hydrophilic black carbon	tavg3_2d_adg_Nx
BCHYPHIL	BCPHOB2PHIL	Conversion of hydrophobic to hydrophilic black carbon	
BCWT001	BCPHOBICWT	Wet deposition of hydrophobic black carbon	tavg3_2d_adg_Nx
BCWT002	BCPHILICWT	Wet deposition of hydrophilic black carbon	tavg3_2d_adg_Nx
NISV001	Combined with NISV002 and NISV003 to NISV	Convective scavenging of nitrate	tavg3_2d_adg_Nx
NISV002	Combined with NISV001 and NISV003 to NISV	Convective scavenging of nitrate	tavg3_2d_adg_Nx
NISV003	Combined with NISV001 and NISV002 to NISV	Convective scavenging of nitrate	tavg3_2d_adg_Nx
OCDP001	OCPHOBICDP	Dry deposition of hydrophobic organic carbon	tavg3_2d_adg_Nx

OCDP002	OCPHILICDP	Dry deposition of hydrophilic organic carbon	tavg3_2d_adg_Nx
OCEM001	OCPHOBICEM	Emissions of hydrophobic organic carbon	tavg3_2d_adg_Nx
OCEM002	OCPHILICEM	Emissions of hydrophilic organic carbon	tavg3_2d_adg_Nx
OCHYPHIL	OCPHOB2PHIL	Conversion of hydrophobic to hydrophilic organic carbon	tavg3_2d_adg_Nx
OCWT001	OCPHOBICWT	Wet deposition of hydrophobic organic carbon	tavg3_2d_adg_Nx
OCWT002	OCPHILICWT	Wet deposition of hydrophilic organic carbon	tavg3_2d_adg_Nx
SUDP001	DMSDP	Dry deposition of dimethyl sulfide	tavg3_2d_adg_Nx
SUDP002	SO2DP	Dry deposition of sulfur dioxide	tavg3_2d_adg_Nx
SUDP003	SO4DP	Dry deposition of sulfate aerosol	tavg3_2d_adg_Nx
SUDP004	MSADP	Dry deposition of methanesulfonic acid	tavg3_2d_adg_Nx
SUEM001	DMSEM	Emissions of dimethyl sulfide	tavg3_2d_adg_Nx
SUEM002	SO2EM	Emissions of sulfur dioxide	tavg3_2d_adg_Nx
SUEM003	SO4EM	Emissions of sulfate aerosol	tavg3_2d_adg_Nx
SUEM004	MSAEM	Emissions of methanesulfonic acid	tavg3_2d_adg_Nx
SUWT001	DMSWT	Wet deposition of dimethyl sulfide	tavg3_2d_adg_Nx
SUWT002	SO2WT	Wet deposition of sulfur dioxide	tavg3_2d_adg_Nx
SUWT003	SO4WT	Wet deposition of sulfate aerosol	tavg3_2d_adg_Nx
SUWT004	MSAWT	Wet deposition of methanesulfonic acid	tavg3_2d_adg_Nx

3. Guidance on the use of PM_{2.5}

The variable PM₂₅ or the total reconstructed dry particulate matter with a geometric diameter smaller than 2.5 microns at the surface can now be found in the *tavg3_2d_aer_Nx* collection. This field is calculated within the model assuming a geometric diameter for aerosol particles and a relative humidity of 0% and the outputted field is defined as

$$PM_{2.5} = DUSMASS25 + SSMASST25 + NISMASST25 + NH4SMASST + SO4SMASST + BCSMASST + OCSMASST + BRSMASST.$$

Note that this definition differs from the recommended calculations for MERRAero and MERRA-2 (Buchard et al., 2017). The conversion of organic carbon to organic matter is already handled within the GOCART-2G model code such that multiplying by 1.4 or 1.8 is not needed. Additionally, the introduction of ammonium as part of the nitrate cycle eliminates the need for converting the sulfate ion to ammonium sulfate. **The formulation given here and included in the *tavg3_2d_aer_Nx* file collection, is not directly comparable to many observations of PM_{2.5} such as those collected by the IMPROVE network or the EPA.** If comparing to observations,

care should be taken such as utilizing a consistent definition of particle diameter and considering the effect of relative humidity on aerosol size. The equation given in Section 3.5 of Collow et al. (2023) can be used to compute PM_{2.5} based on an aerodynamic diameter and a specified relative humidity using fields in the *inst3_3d_aer_Nv* collection.

4. Science Impacts of GOCART-2G

Intentional changes were made in GOCART-2G related to the code itself and the selection of emissions that will impact the relative contributions of aerosol species to the total AOD within GEOS. Impacts of these changes are evaluated within this section using three configurations of GEOS as described in Table 3. GEOS-FPP represents a candidate system that was used for evaluating the implementation of GOCART-2G for use in the next GEOS-FP system. In addition to changes pertaining to aerosols, differences between GEOS-FPP and GEOS-FP version 5.29.5 (the current version of GEOS-FP as of January 2026) include modifications in the assimilated meteorological observations, a more recent version of the Community Radiative Transfer Model (CRTM), and a refactoring of the moist processes code. Testing was performed with GEOS ADAS version 5.42.1, while the next GEOS-FP is based on GEOS ADAS 5.43.0. However, any change associated with this version update to GEOS ADAS can be considered negligible. GEOS-IT is a lower resolution near-real time product intended for instrument teams and is included as an additional data point due to its use of the newer anthropogenic emissions however this system utilizes the legacy version of the GOCART code (<https://gmao.gsfc.nasa.gov/gmao-products/geos-it/>).

Table 3. Summary of simulations evaluated in this document.

	GEOS-FPP	GEOS-FP	GEOS-IT
GEOS ADAS Version	5.42.1	5.29.5-p6	5.29.4
GEOS GCM Version	11.7.0	10.19	10.19
GOCART Version	2.3	1.0.2	1.0.2
Spatial Resolution	~12 km	~12 km	~50 km
Meteorology Data Assimilation	Hybrid 4D-EnVar, all sky (Todling and El Akkraoui, 2018)	Hybrid 4D-EnVar, all sky (Todling and El Akkraoui, 2018)	3D Var, clear sky (Todling and El Akkraoui, 2018)
Aerosol Data Assimilation	PSAS + LDE*, MODIS NNR AOD at 550 nm + AERONET (Randles et al., 2017)	PSAS + LDE*, MODIS NNR AOD at 550 nm + AERONET (Randles et al., 2017)	PSAS + LDE*, MODIS NNR AOD at 550 nm + AERONET (Randles et al., 2017)
Anthropogenic Emissions	CEDS v202104 (corrected seasonal cycle)	HTAP v2.2	CEDS v202104
Biomass Burning Emissions	QFED 2.6r1 * 0.778	QFED 2.6r1	QFED 2.6r1
Volcanic Emissions	Carn	None	None

Prescribed Precursor Gases/Oxidants	MERRA-2 GMI (2019)	MERRA GMI (2010)	MERRA-2 GMI (2019)
Biogenic Emissions	MEGAN	GEIA (Guenther et al., 1995)	GEIA (Guenther et al., 1995)

*PSAS+LDE = Physical-space Statistical Analysis System with Local Displacement Ensemble

4.1 Emissions

GOCART-2G allows for prescribed emissions from varying sources including biomass burning, volcanoes, anthropogenic sources, and other natural sources like biogenic VOCs, which are summarized in Table 3. In the following tests, biomass burning emissions have not changed between GEOS-FP and GEOS-FPP and still come from the Quick Fire Emissions Dataset (QFED) version 2.6r1 (Darmenov and da Silva, 2015). GOCART-2G introduced degassing volcanic emissions of sulfur dioxide (SO₂) in GEOS-FPP. Degassing emissions are a monthly climatology derived from the time series of degassing emissions provided by Carn et al. (2017) over the period of 2005 through 2019. As a near real time system that produces forecasts, GEOS currently does not have a mechanism to include explosive eruptions or updates to the degassing sources. Biogenic emissions have also been included for the first time, and this is as described in the Supplement of Collow et al. (2024).

GEOS-FP used anthropogenic emissions from the Hemispheric Transport of Air Pollution (HTAP) version 2.2 for the year 2010 (Janssens-Maenhout et al., 2015). These emissions are out of date and are not representative of changes in emission patterns that have occurred over the past decade. As a result, the present study has switched to year 2019 of the 2021 release of the Community Earth atmospheric Data System (CEDS; Hoesly et al., 2018). These anthropogenic emissions are similar to those used for GEOS-IT however a correction to the seasonal cycle was applied (Hoesly et al., 2025). The CEDS dataset includes spatially varying monthly values of anthropogenic emissions that undergo a temporal interpolation to daily values within GEOS. Prescribed gaseous precursors, hydroxide (OH), hydrogen peroxide (H₂O₂), and nitric acid (HNO₃), are taken from the MERRA-2 Global Modeling Initiative (GMI) simulation (Strode et al., 2019) instead of an older GMI simulation that used meteorology from MERRA (referred to as GEOSCCM in Lamarque et al., 2013).

Figure 1 shows time series of the total global anthropogenic emissions of SO₂, ammonia (NH₃), organic carbon, and black carbon as used for GEOS-FP, GEOS-FPP, and GEOS-IT. On an annual basis, GEOS-FPP and GEOS-IT emissions are identical for each species, however they have opposite seasonal cycles. The more modern emissions dataset used for GEOS-FPP and GEOS-IT has a decrease in SO₂ emissions compared to GEOS-FP, dropping the annual total emissions of SO₂ from 1.3 Tg to 1.0 Tg (Figure 1a). This decrease predominantly occurs over China and India, and to a lesser extent, over the eastern United States and Europe. Ammonia emissions have increased slightly, however the more notable difference between HTAP and CEDS is the seasonal cycle. HTAP has a more muted seasonal cycle for ammonia emissions while CEDS includes large maxima during the boreal spring and fall months for agricultural applications of fertilizer (Figure 1b). The change in character in ammonia emissions between all three versions of GEOS has the potential to create significant differences in temporal and spatial patterns in nitrate aerosol. Black and organic carbon emissions have increased with regards to the annual total, and the emissions used for GEOS-FP have a smaller amplitude of the seasonal cycle.

Global Total Anthropogenic Emissions

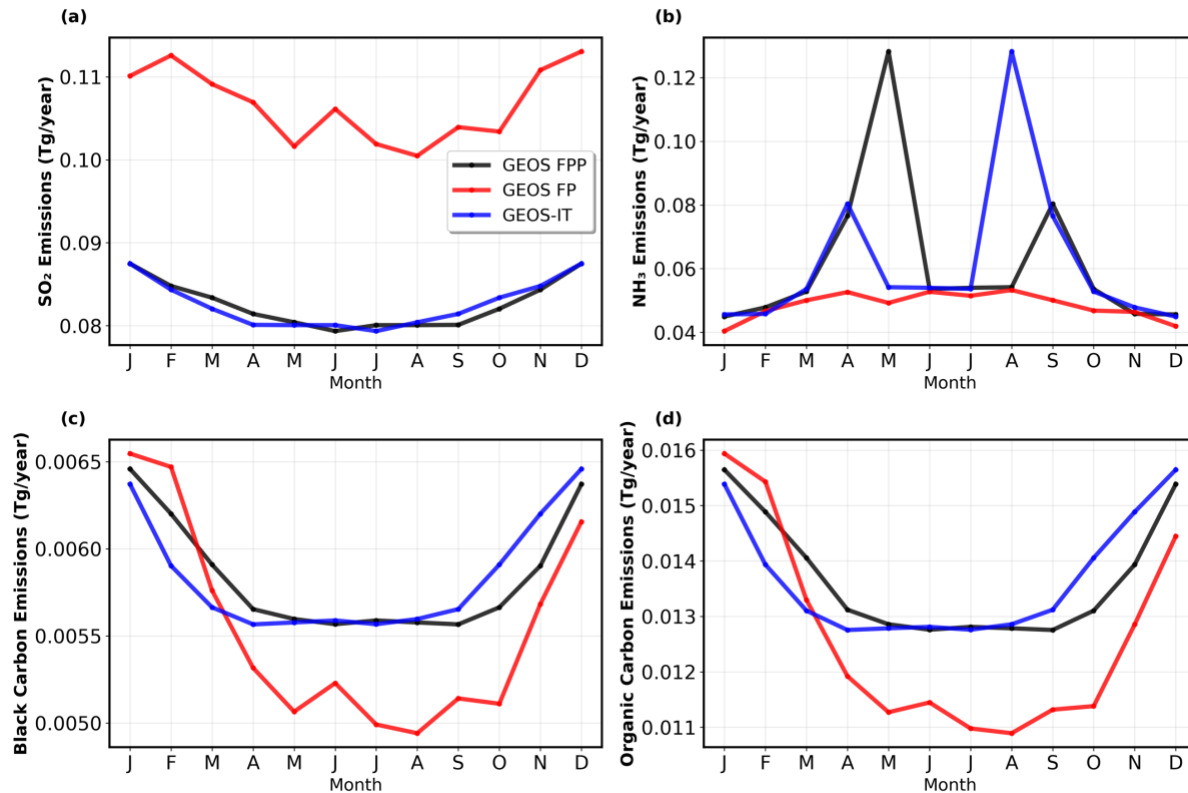


Figure 1: Anthropogenic emissions of (a) sulfur dioxide, (b) ammonia, (c) black carbon, and (d) organic carbon used for GEOS-FPP, GEOS-FP, and GEOS-IT.

4.2 Total Aerosol Optical Depth

Figure 2 shows spatial maps of the mean total AOD at 550 nm in GEOS-FPP, GEOS-FP, and GEOS-IT for the period of April through July 2025. The spatial pattern for the total AOD is in excellent agreement between the three systems. A time series of the total AOD for April through July of 2025 can be found in Figure 3. The total AOD at 550 nm in GEOS-FPP is slightly higher than the other two systems however they are still highly correlated with $R=0.976$ for GEOS-FP and $R=0.982$ for GEOS-IT (Figure 4a and b). Each system captures an increase in total AOD during the month of June due to Canadian wildfires and plumes of dust being transported across the Atlantic. All three GEOS systems are so similar because they all assimilate the same observations of total AOD at 550 nm from surface AERONET observations as well as and neural net retrievals (NNR) applied to satellite observation from MODIS aboard Aqua and Terra. The assimilation can behave in slightly different manners, resulting in different values for total AOD, as the background state will change due to changes in the emissions, underlying meteorology, and version of GOCART.

Total AOD at 550 nm for April-July 2025

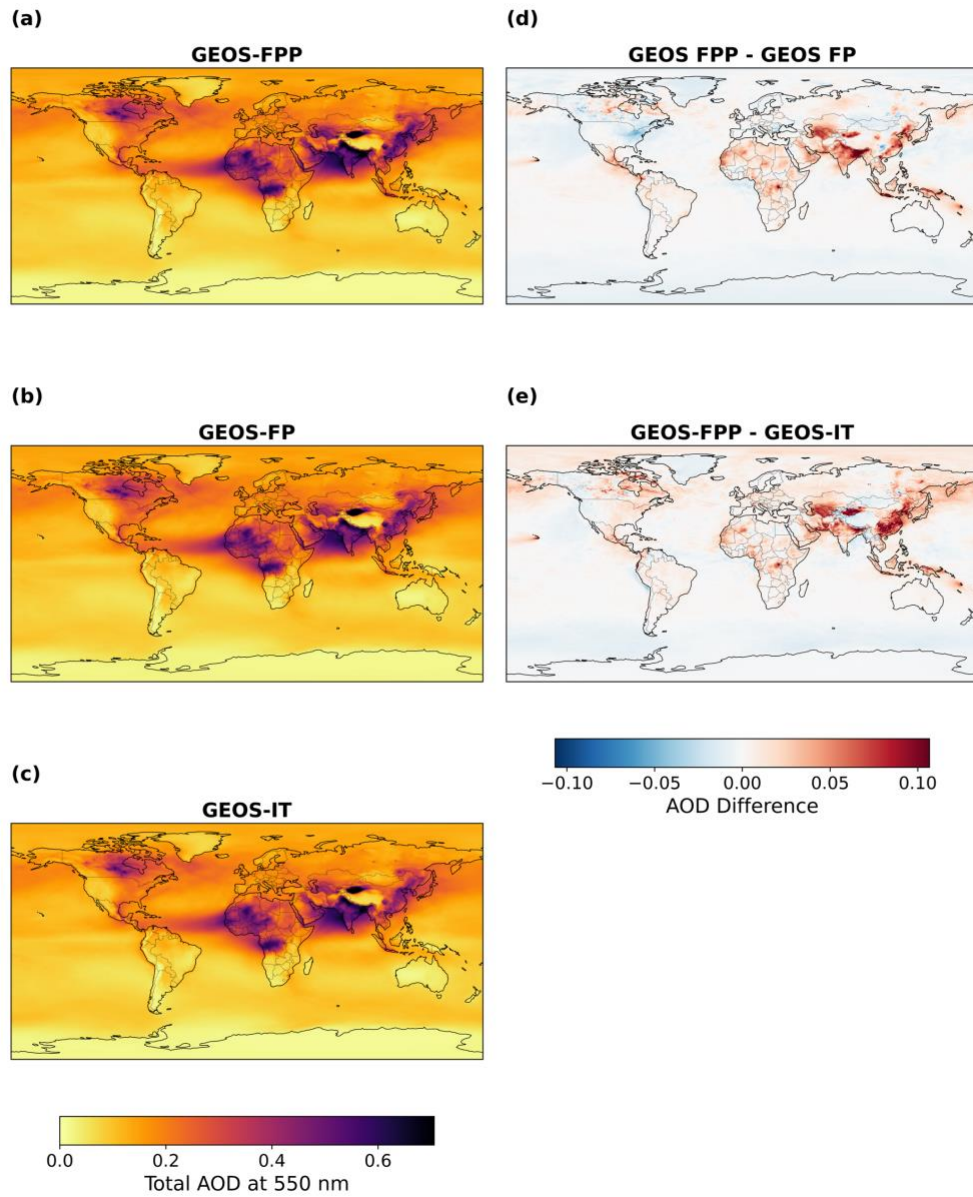


Figure 2: Total aerosol optical depth (AOD) at 550 nm averaged over April through July 2025 in (a) GEOS-FPP, (b) GEOS-FP, and (c) GEOS-IT and the difference between (d) GEOS-FPP and GEOS-FP and (e) GEOS-FPP and GEOS-IT.

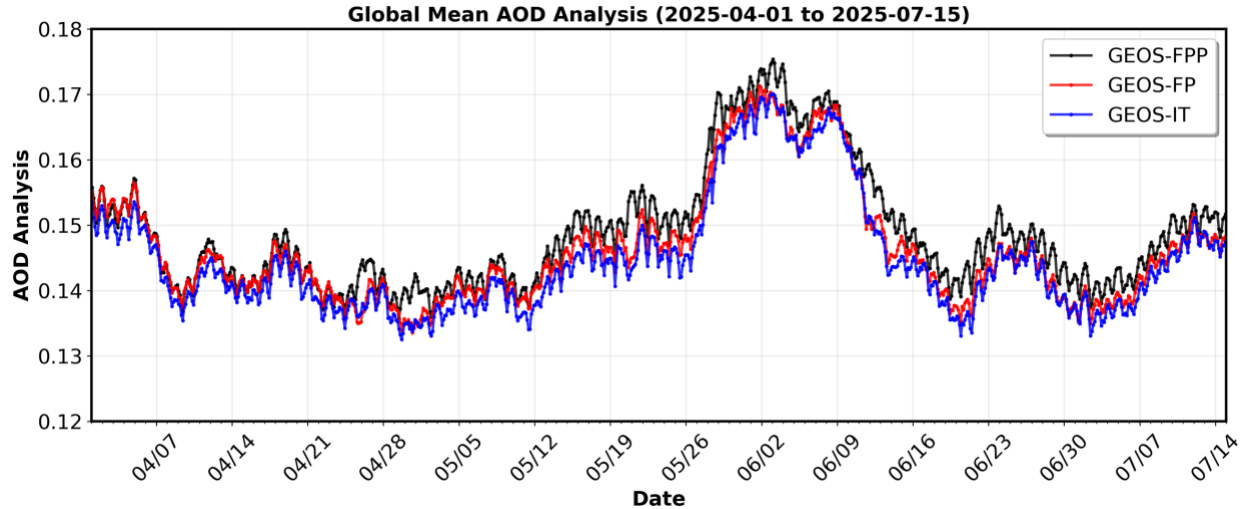


Figure 3: Timeseries of the global mean 3-hourly total aerosol optical depth (AOD) at 550 nm for the period of April 1, 2025 through July 15, 2025 from GEOS-FPP(black), GEOS-FP (red), and GEOS-IT (blue).

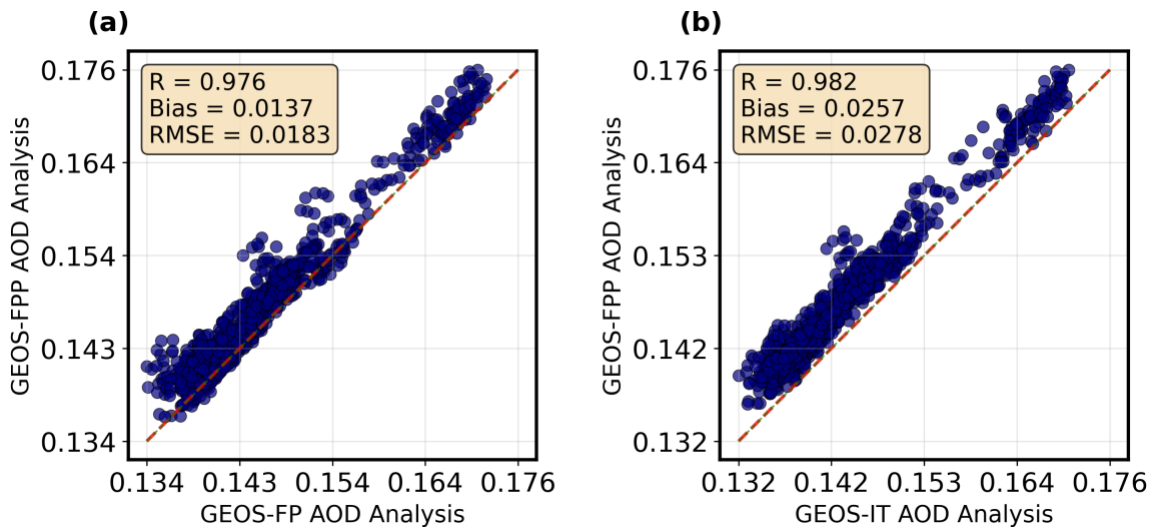


Figure 4: Scatter plots of global mean 3-hourly total aerosol optical depth (AOD) at 550 nm comparing GEOS-FPP to (a) GEOS-FP and (b) GEOS-IT as $\log(\text{AOD}+0.01)$ for the period of April 1, 2025 through July 15, 2025. The red dashed line in each panel represents the one-to-one line. R is the Pearson correlation coefficient, bias is computed as the mean difference, and RMSE is the root mean square error computed as $\log(\text{AOD}+0.01)$.

It is important to remember that the observations only constrain the total AOD. More uncertainty exists with the aerosol speciation and that is entirely dependent on the aerosol model and prescribed emissions. The total AOD is broken into contributions from individual species in Figures 5 through 10. The color bars in panel (a) for each figure intentionally use the same range to highlight which species have changed the most between the legacy GOCART code and

GOCART-2G. In the following, we will review the impacts of the updates to GEOS-FPP on each species.

4.3 Organic, Brown, and Black Carbon

The largest scientific change in GOCART-2G impacts organic carbon, which was split in GEOS-FPP into the anthropogenic (OC) and biomass burning (BR) components. These two components are treated in an identical manner for transport and removal however brown carbon uses a different optics look up table that is more absorbing at wavelengths shorter than 550 nm (Colarco et al., 2017). In order to facilitate direct comparisons between GEOS-FP, GEOS-IT and GEOS-FPP (the first two of which do not contain BR), in the comparisons below we sum the OC and BR components in GEOS-FPP to get a "total" organic carbon burden. The AOD for total organic carbon has increased globally in GEOS-FPP with the largest increases occurring over land (Figure 5a-d). While the introduction of secondary organic aerosols from biogenic sources plays a role, the predominant factor in the increase of organic carbon AOD is summertime increase in anthropogenic organic carbon emissions. An increase in the ratio that converts emitted organic carbon to organic aerosol particulate matter (POM) from 1.4 to 1.8 to better align with observations from recent field campaigns (Hodzic et al. 2020), is also a contributing factor to the increase in organic carbon in GEOS-FPP. Despite the increase in the total organic carbon AOD, the global means are very highly correlated between GEOS-FPP, GEOS-FP, and GEOS-IT. To compensate for the additional particulate organic matter, biomass burning emissions were scaled down to 78%. This scaling was uniformly applied to species emitted from biomass burning including brown carbon, black carbon, sulfur dioxide, and ammonia. Aside from differences that can arise from the AOD assimilation, the reduction in biomass burning emissions is the only difference in black carbon between GEOS-FPP, GEOS-FP, and GEOS-IT and results in a slightly lower AOD for black carbon in GEOS-FPP (Figure 6).

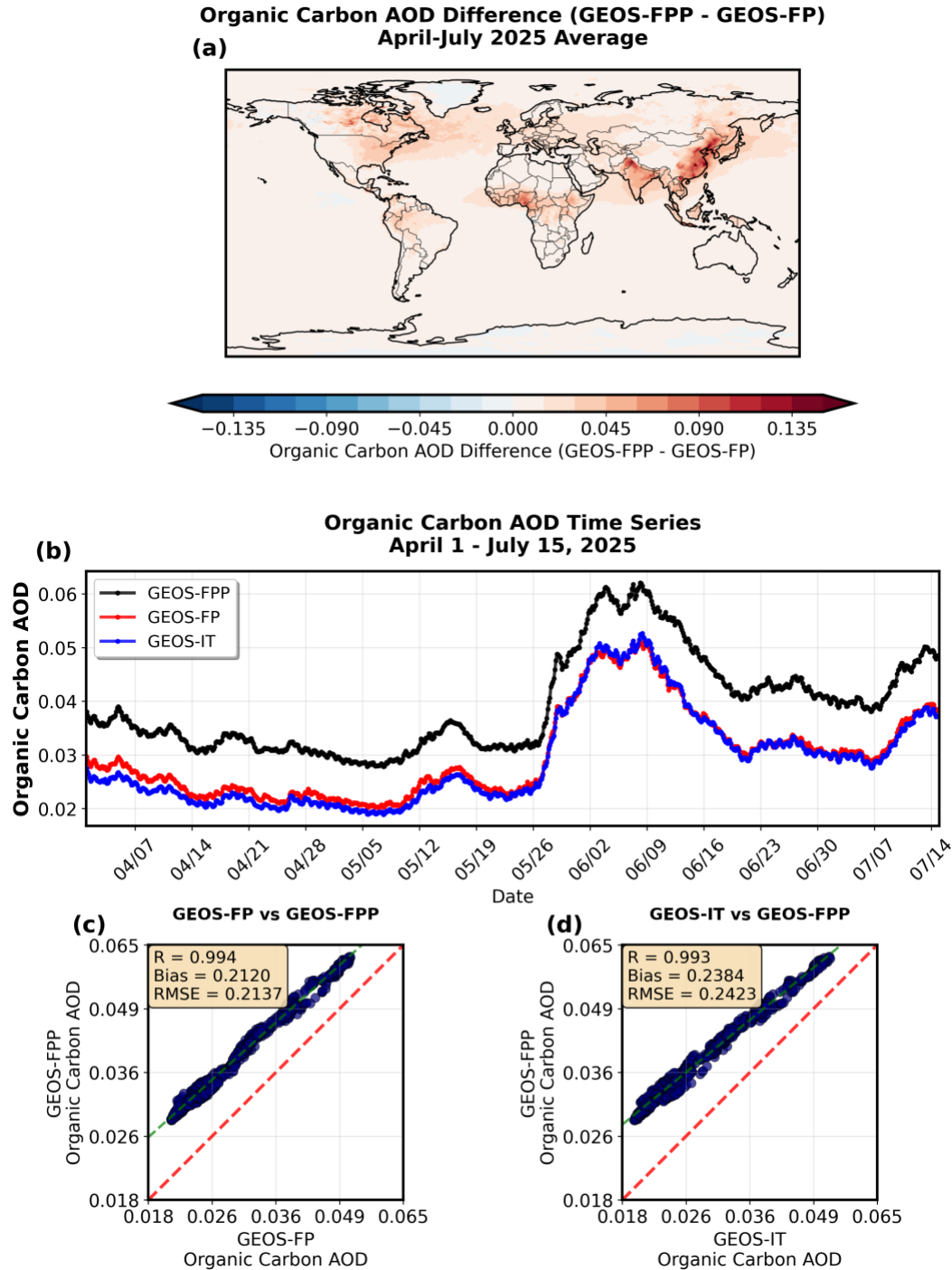


Figure 5: (a) Spatial map of the difference in total organic carbon aerosol optical depth (AOD) for the April through July 2025 displayed as GEOS-FPP minus GEOS-FP. (b) Time series of 3-hourly global mean total organic carbon AOD for the period of April 1, 2025 through July 15, 2025 for GEOS-FPP (black), GEOS-FP (red), and GEOS-IT (blue). (c) Scatter plot of 3-hourly global mean total organic carbon AOD for GEOS-FPP against GEOS-FP as $\log(\text{AOD} + 0.01)$. (d) Scatter plot of 3-hourly global mean total organic carbon AOD for GEOS-FPP against GEOS-IT as $\log(\text{AOD} + 0.01)$. The dashed red line in (c) and (d) represents the one-to-one line while the dashed light blue line represents the linear fit.

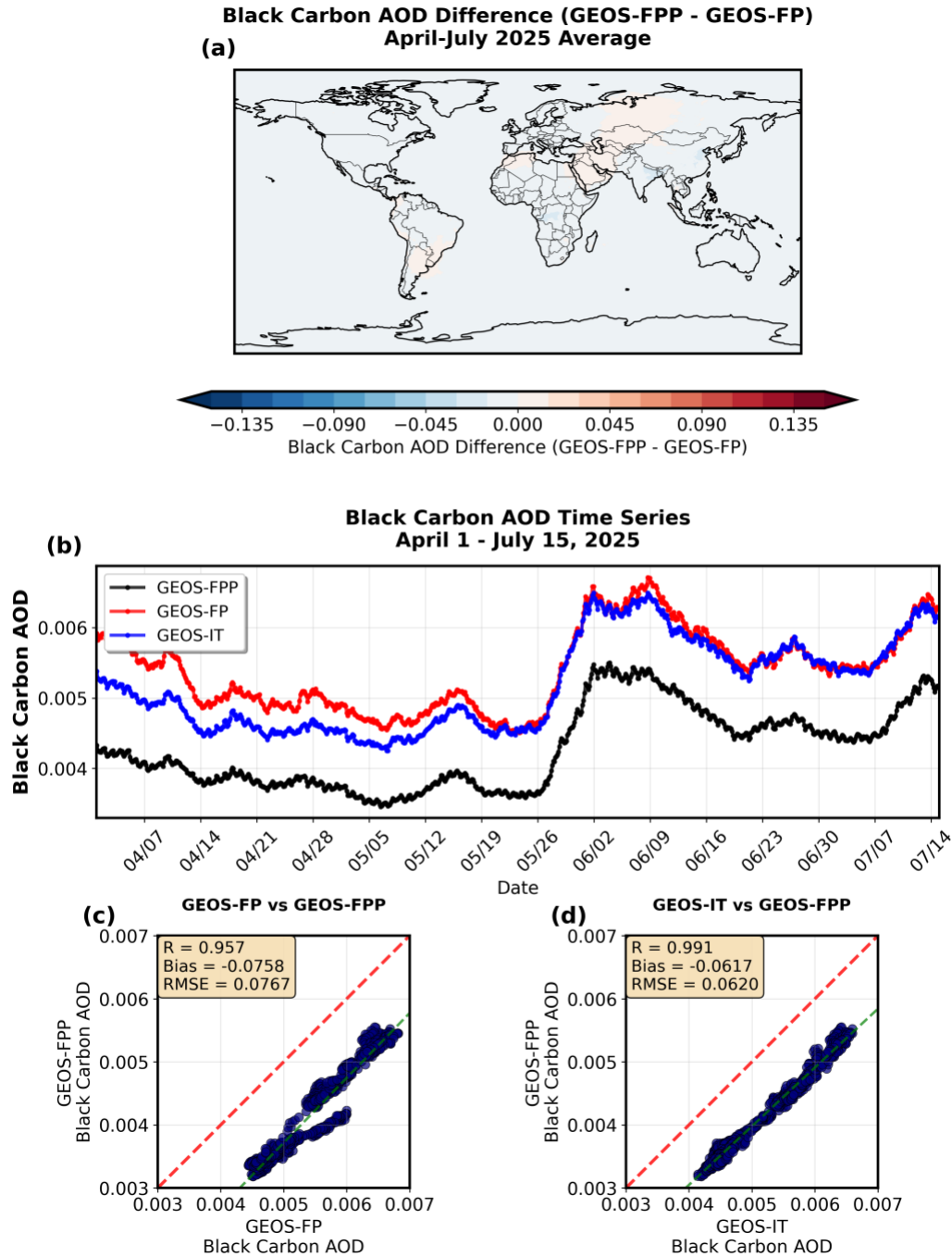


Figure 6: (a) Spatial map of the difference in black carbon aerosol optical depth (AOD) for April through July 2025 displayed as GEOS-FPP minus GEOS-FP. (b) Time series of 3-hourly global mean black carbon AOD for the period of April 1, 2025 through July 15, 2025 for GEOS-FPP (black), GEOS-FP (red), and GEOS-IT (blue). (c) Scatter plot of 3-hourly global mean black carbon AOD for GEOS-FPP against GEOS-FP as $\log(\text{AOD}+0.01)$. (d) Scatter plot of 3-hourly global mean black carbon AOD for GEOS-FPP against GEOS-IT as $\log(\text{AOD}+0.01)$. The dashed red line in (c) and (d) represents the one-to-one line while the dashed light blue line represents the linear fit.

4.4 Sulfate

Sulfate is produced from anthropogenic and natural emissions of SO₂ and has been impacted in GEOS-FPP by changes in the emissions datasets as discussed in Section 4. No additional changes were made to the model code for GOCART-2G pertaining to sulfate. However, changes in the oxidant fields that drive sulfate formation will have small impacts secondary to emissions changes. Anthropogenic emissions of SO₂ have decreased over the past decade, and this is noticeable in the difference in sulfate AOD between GEOS-FPP and GEOS-FP over China, India, and the eastern United States (Figure 7a). Increases in sulfate AOD can be seen across the tropics, particularly in the tropical western Pacific, central Africa, central America, and near Hawaii. These are all locations with volcanic activity that is being represented in GEOS-FPP with a climatology of degassing volcanic emissions. Neither GEOS-FP nor GEOS-IT include volcanic emissions for the year 2025. Since GEOS-IT does not have volcanic emissions but uses the more recent anthropogenic emissions and GEOS-FP uses an outdated data set for anthropogenic emissions, the global mean sulfate AOD for GEOS-FPP falls in between the other two systems. The temporal correlations between GEOS-FPP, GEOS-FP, and GEOS-IT are weaker than for other aerosol species, however the time series generally follow the same pattern (Figure 7b-d).

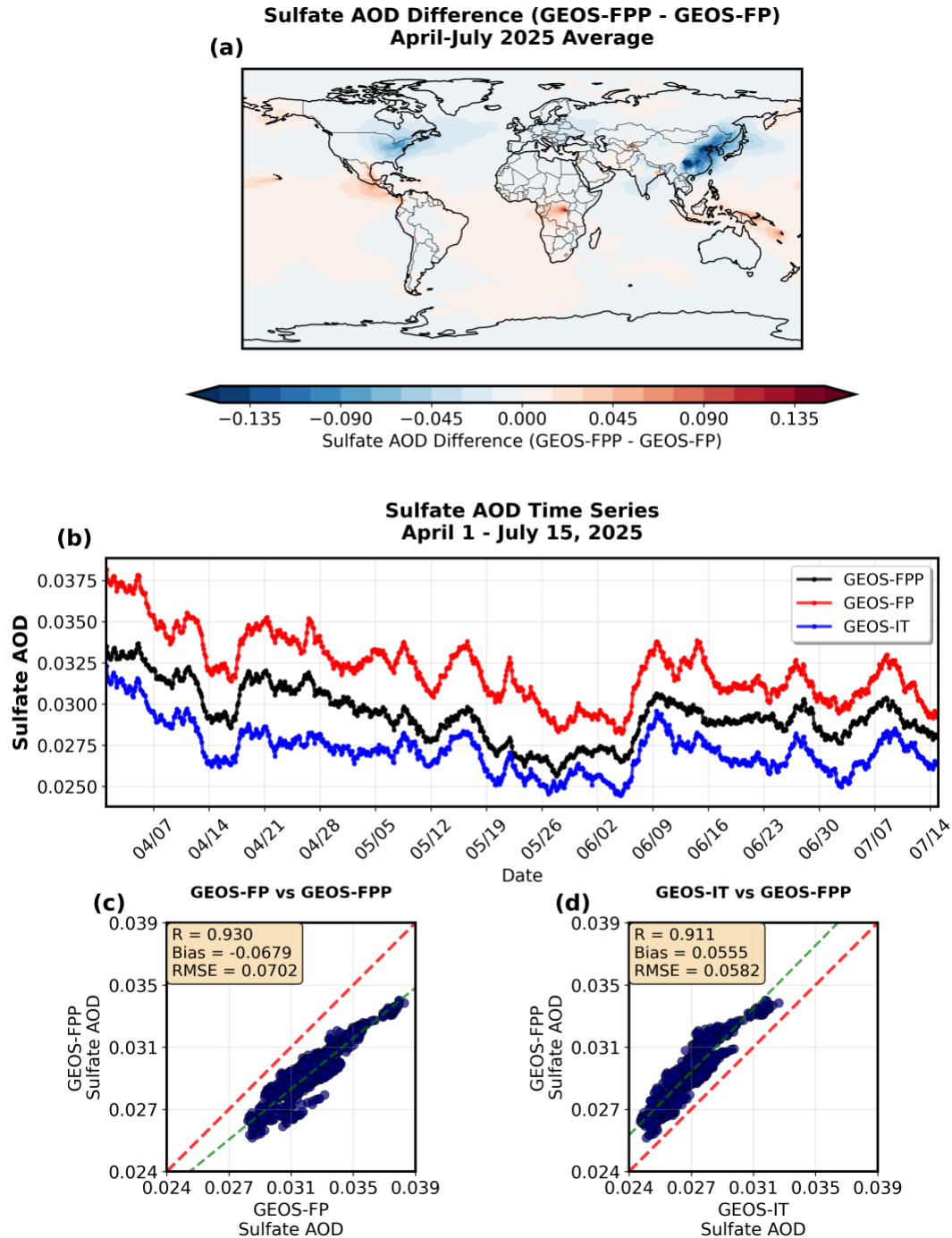


Figure 7: (a) Spatial map of the difference in sulfate aerosol optical depth (AOD) for April through July 2025 displayed as GEOS-FPP minus GEOS-FP. (b) Time series of 3-hourly global mean sulfate AOD for the period of April 1, 2025 through July 15, 2025 for GEOS-FPP (black), GEOS-FP (red), and GEOS-IT (blue). (c) Scatter plot of 3-hourly global mean sulfate AOD for GEOS-FPP against GEOS-FP as $\log(\text{AOD}+0.01)$. (d) Scatter plot of 3-hourly global mean sulfate AOD for GEOS-FPP against GEOS-IT as $\log(\text{AOD}+0.01)$. The dashed red line in (c) and (d) represents the one-to-one line while the dashed light blue line represents the linear fit.

4.5 Nitrate

Nitrate is also impacted by changes in the anthropogenic emissions dataset, in addition to the selection of the MERRA-2 GMI dataset for prescribing the precursor gas, nitric acid. Nitrate AOD has increased in GEOS-FPP compared to GEOS-FP, with the largest increases over China, India, and Nepal (Figure 8a). Over southeast Asia, additional nitrate is produced through aqueous and heterogenous processes from precursor gases including ammonia and nitric acid, both of which are more prevalent in GEOS-FPP due to the selection of emissions and prescribed nitric acid. Using the spring and early summer months for the test case of GEOS-FPP highlights the differences in the seasonal cycle of the emissions. The older HTAP dataset does not include a seasonal cycle for ammonia, while the version of CEDS used for GEOS-FPP has a large peak in May. As a result, there is no temporal correlation in the global mean time series between GEOS-FPP, GEOS-FP, or GEOS-IT (Figure 8b-d). Had the test case instead looked at November through February, the timeseries would likely be correlated as there are no peaks in emissions due to farming practices in those months. One minor change that resulted from bug fixes in aqueous nitrate production in GOCART-2G that can be seen in the timeseries is a larger amplitude in the diurnal cycle in global mean nitrate AOD. This is associated with larger swings in the production and loss of nitrate through aqueous processes.

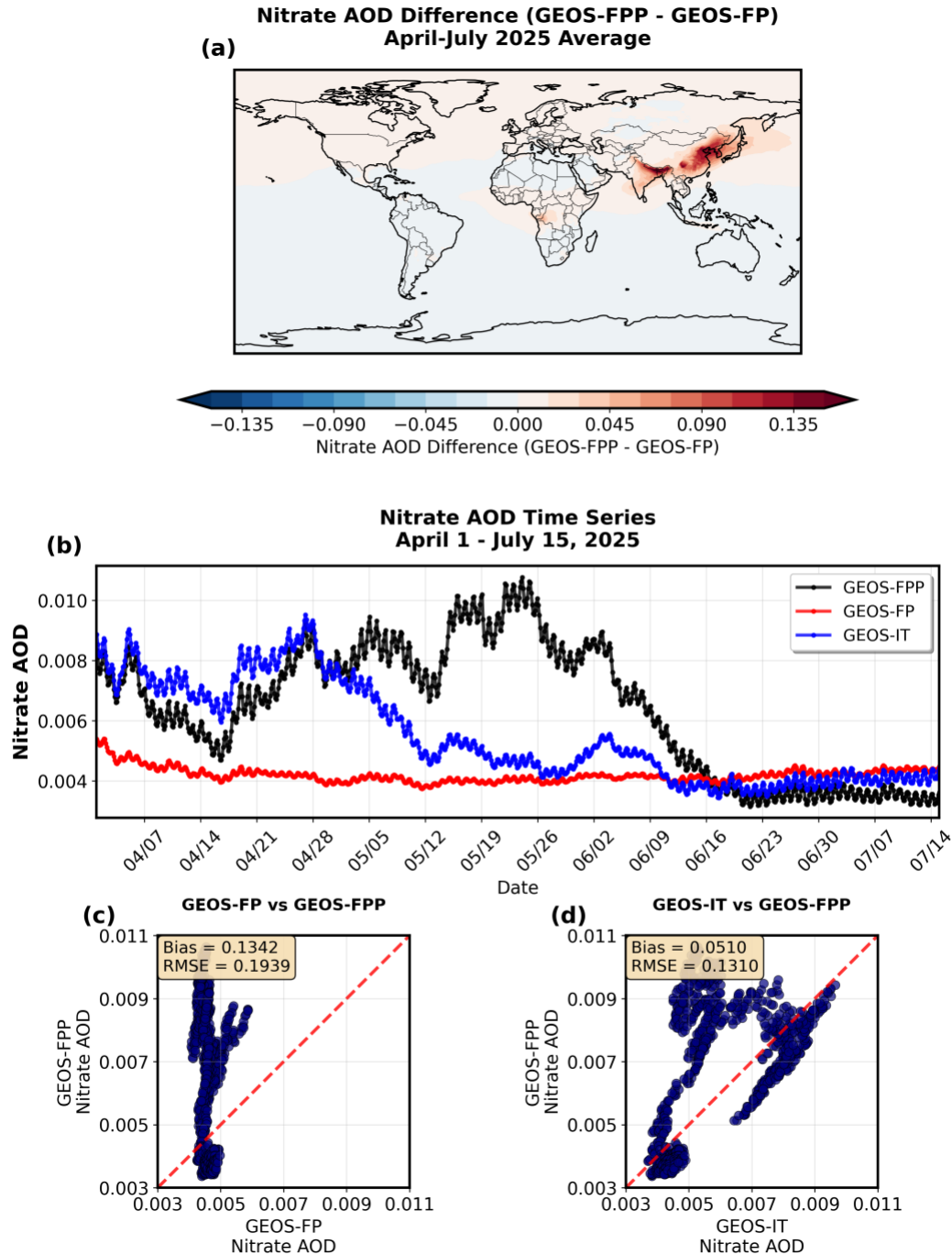


Figure 8: (a) Spatial map of the difference in nitrate aerosol optical depth (AOD) for April through July 2025 displayed as GEOS-FPP minus GEOS-FP. (b) Time series of 3-hourly global mean nitrate AOD for the period of April 1, 2025 through July 15, 2025 for GEOS-FPP (black), GEOS-FP (red), and GEOS-IT (blue). (c) Scatter plot of 3-hourly global mean nitrate AOD for GEOS-FPP against GEOS-FP as $\log(\text{AOD}+0.01)$. (d) Scatter plot of 3-hourly global mean nitrate AOD for GEOS-FPP against GEOS-IT as $\log(\text{AOD}+0.01)$. The dashed red line in (c) and (d) represents the one-to-one line while the dashed light blue line represents the linear fit.

4.6 Sea Salt

There were no deliberate changes for sea salt as part of GOCART-2G as evidenced by the difference map between GEOS-FPP and GEOS-FP (Figure 9a). Global mean sea salt AOD in GEOS-FPP is highly correlated with the global means for GEOS-FP and GEOS-IT (Figure 9 b-d). There is a slight inclination for the global mean sea salt AOD to be lower in magnitude in GEOS-FPP compared to GEOS-FP, particularly during the months of May, June, and July (Figure 9b and d). This is most likely related to the AOD assimilation balancing the available aerosol species to bring the model closer to the MODIS observations and will be discussed in more depth later. GEOS-IT stands out for having the largest global mean sea salt AOD, and this mainly occurs over the Southern Ocean and tropical western Pacific. While the underlying model is the same between GEOS-IT and GEOS-FP, the resolution is coarser, and the meteorological data assimilation uses a more basic approach to reduce the necessary computing resources. These meteorological configuration choices impact convection and precipitation, which ultimately impacts wind-driven sea salt emission and deposition.

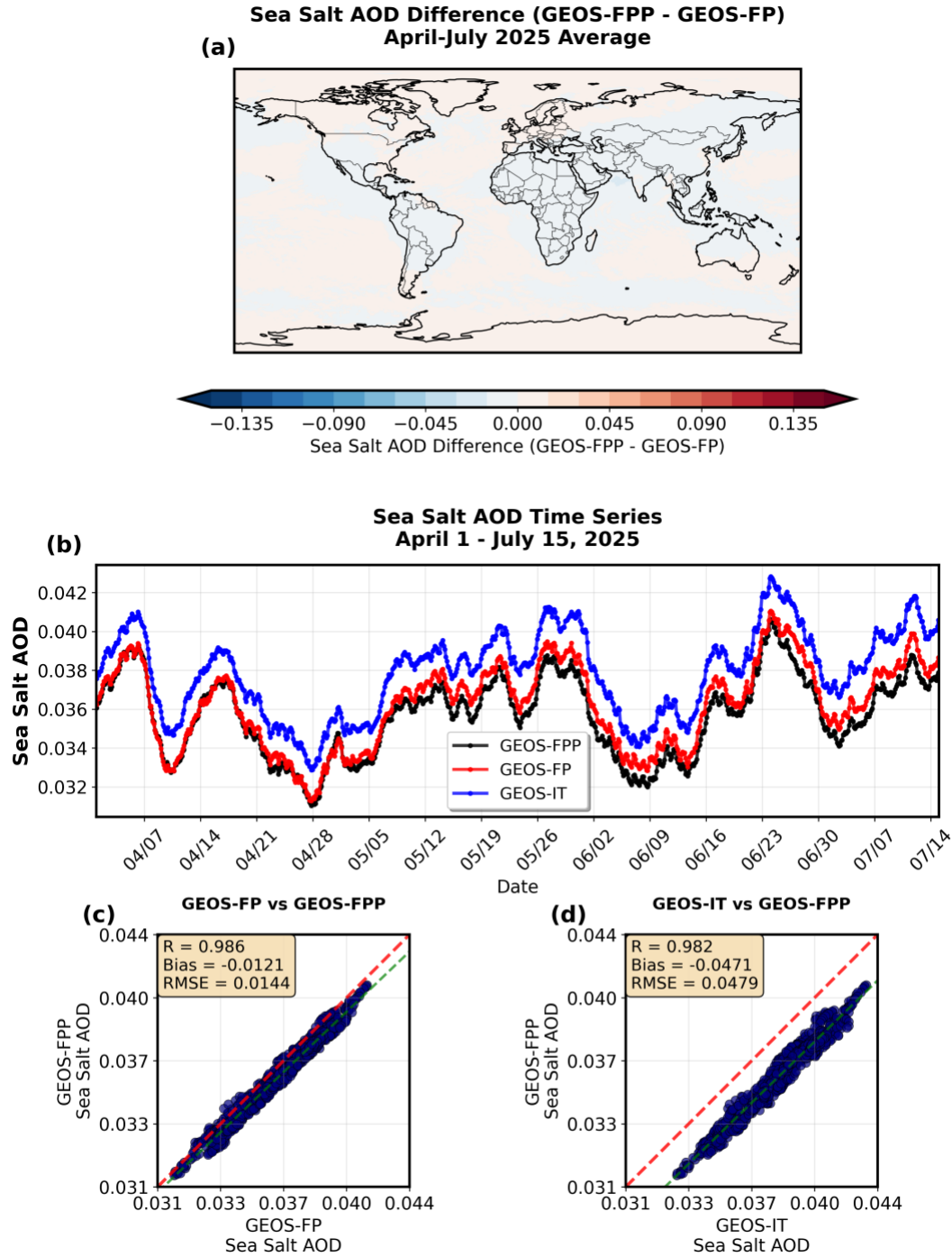


Figure 9: (a) Spatial map of the difference in sea salt aerosol optical depth (AOD) for April through July 2025 displayed as GEOS-FPP minus GEOS-FP. (b) Time series of 3-hourly global mean sea salt AOD for the period of April 1, 2025 through July 15, 2025 for GEOS-FPP (black), GEOS-FP (red), and GEOS-IT (blue). (c) Scatter plot of 3-hourly global mean sea salt AOD for GEOS-FPP against GEOS-FP as $\log(\text{AOD}+0.01)$. (d) Scatter plot of 3-hourly global mean sea salt AOD for GEOS-FPP against GEOS-IT as $\log(\text{AOD}+0.01)$. The dashed red line in (c) and (d) represents the one-to-one line while the dashed light blue line represents the linear fit.

4.7 Dust

Like with sea salt, dust emissions are parameterized as a function of the modeled near surface wind speed. Little was changed in the model code for dust in moving from legacy GOCART to GOCART-2G, however it has been noted that GOCART-2G results in increased dust emissions (Collow et al., 2024). This feature can be seen in the spatial map in Figure 10a, depicting the difference in dust AOD between GEOS-FPP and GEOS-FP. Over dusty regions including northern Africa, Saudi Arabia, the Taklamakan desert, and to a lesser extent, Australia, there is a larger dust AOD in GEOS-FPP. Elsewhere, the dust AOD has decreased between GEOS-FP and GEOS-FPP resulting in a global mean dust AOD that is lower in GEOS-FPP than GEOS-FP and GEOS-IT. This decrease is in response to the ratio of each aerosol species within the AOD data assimilation. When the assimilation occurs, aerosol mass will either be added or subtracted from individual species to bring the total AOD closer to the observations, but it is done so according to what aerosols are present in the background state. In this situation there is a larger proportion of organic and brown carbon to the total aerosol mass in GEOS-FPP compared to the other two systems, and the aerosol assimilation may be apportioning more of the analysis increment to carbon species in this system.

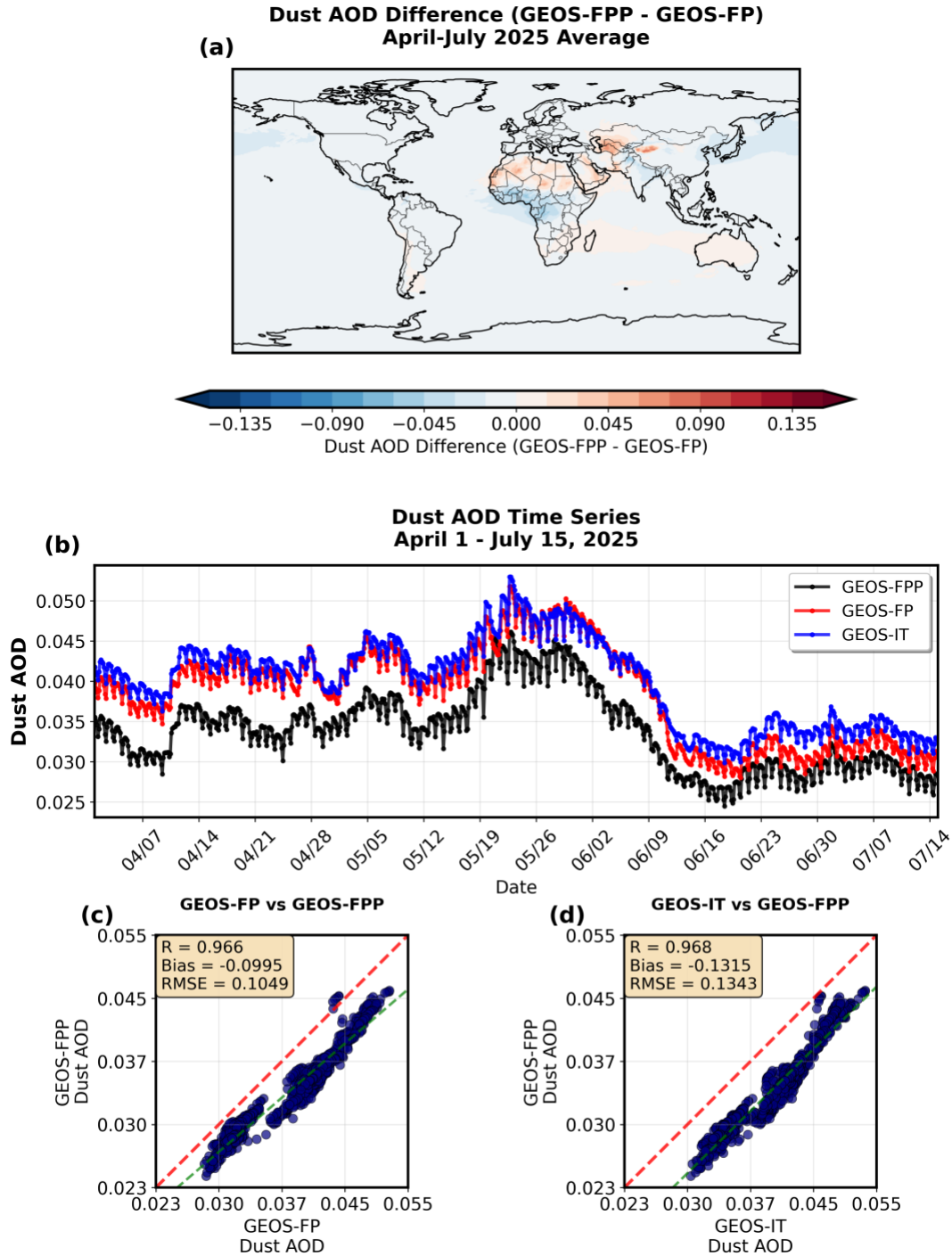


Figure 10: (a) Spatial map of the difference in dust aerosol optical depth (AOD) for April through July 2025 displayed as GEOS-FPP minus GEOS-FP. (b) Time series of 3-hourly global mean dust AOD for the period of April 1, 2025 through July 15, 2025 for GEOS-FPP (black), GEOS-FP (red), and GEOS-IT (blue). (c) Scatter plot of 3-hourly global mean dust AOD for GEOS-FPP against GEOS-FP as $\log(\text{AOD}+0.01)$. (d) Scatter plot of 3-hourly global mean dust AOD for GEOS-FPP against GEOS-IT as $\log(\text{AOD}+0.01)$. The dashed red line in (c) and (d) represents the one-to-one line while the dashed light blue line represents the linear fit.

Summary

The introduction of GOCART-2G in GEOS-FP 5.43.0 was a necessary step for future development of aerosols within GEOS. The associated changes have the potential to impact users depending on the application. Due to the assimilation of observed 550 nm AOD, there are minimal impacts on the total aerosol optical depth. There are, however, changes in the relative proportions of each aerosol species in response to code changes made for organic carbon as well as the selections made for anthropogenic emissions, oxidant fields, and volcanic emissions. Additional variables have been added to the GEOS-FP file specification, as detailed in section 2. For the first time, surface particulate matter smaller than 2.5 microns (PM_{2.5}) is available from GEOS-FP beginning with version 5.43.0, but it is important to consider whether this formulation for PM_{2.5} is appropriate for a given application.

Acknowledgements

Implementing GOCART-2G was a large group effort that would not have been possible without the contributions from numerous people within the GMAO including the software infrastructure team and well as the operations and monitoring groups. We would also like to thank Pete Colarco and our colleagues in the Atmospheric Chemistry and Dynamics Laboratory for valuable discussions along the way.

References

- Buchard, V., Randles, C. A., da Silva, A. M., Darmenov, A., Colarco, P. R., Govindaraju, R., Ferrare, R., Hair, J., Beyersdorf, A. J., Ziemba, L. D., and Yu, H.: The MERRA-2 Aerosol Reanalysis, 1980 Onward. Part II: Evaluation and Case Studies, *J. Climate*, 30, 6851–6872, <https://doi.org/10.1175/JCLI-D-16-0613.1>, 2017.
- Carn, S. A., Fioletov, V. E., McLinden, C. A., Li, C., and Krotkov, N. A.: A decade of global volcanic SO₂ emissions measured from space, *Sci. Rep.*, 7, 44095, <https://doi.org/10.1038/srep44095>, 2017.
- Colarco, P. R., Gassó, S., Ahn, C., Buchard, V., da Silva, A. M., and Torres, O.: Simulation of the Ozone Monitoring Instrument aerosol index using the NASA Goddard Earth Observing System aerosol reanalysis products, *Atmos. Meas. Tech.*, 10, 4121–4134, <https://doi.org/10.5194/amt-10-4121-2017>, 2017.
- Collow, A., V. Buchard, M. Chin, P. Colarco, A. Darmenov, and A. da Silva: Supplemental Documentation for GEOS Aerosol Products. GMAO Office Note No. 22 (Version 1.1), 8 pp, <https://gmao.gsfc.nasa.gov/media/publications/zbly36ziNFDFbmYmvhQeVqPhUo/Collow1489.pdf>, 2023.
- Collow, A. B., Colarco, P. R., da Silva, A. M., Buchard, V., Bian, H., Chin, M., Das, S., Govindaraju, R., Kim, D., and Aquila, V.: Benchmarking GOCART-2G in the Goddard Earth Observing System (GEOS), *Geosci. Model Dev.*, 17, 1443–1468, <https://doi.org/10.5194/gmd-17-1443-2024>, 2024.

Darmenov, A. and da Silva, A.: The quick fire emissions dataset (QFED) – Documentation of versions 2.1, 2.2 and 2.4. NASA//TM-2015-104606, Vol. 38, NASA Global Modeling and Assimilation Office, 183 pp., <https://gmao.gsfc.nasa.gov/pubs/docs/Darmenov796.pdf>, 2015.

Guenther, A., Hewitt, N., Erickson, D., Fall, R., Geron, C., Graedel, T., Harley, P., Klinger, L., Lerdau, M., McKay, W., Pierce, T., Scholes, B., Steinbrecher, R., Tallamraju, R., Taylor, J., and Zimmerman, P.: A global model of natural volatile organic compound emissions, *J. Geophys. Res.*, 100, 8873–8892, 1995.

Hodzic, A., Campuzano-Jost, P., Bian, H., Chin, M., Colarco, P. R., Day, D. A., Froyd, K. D., Heinold, B., Jo, D. S., Katich, J. M., Kodros, J. K., Nault, B. A., Pierce, J. R., Ray, E., Schacht, J., Schill, G. P., Schroder, J. C., Schwarz, J. P., Sueper, D. T., Tegen, I., Tilmes, S., Tsigaridis, K., Yu, P., and Jimenez, J. L.: Characterization of organic aerosol across the global remote troposphere: a comparison of ATom measurements and global chemistry models, *Atmos. Chem. Phys.*, 20, 4607–4635, <https://doi.org/10.5194/acp-20-4607-2020>, 2020.

Hoesly, R. M., Smith, S. J., Feng, L., Klimont, Z., Janssens-Maenhout, G., Pitkanen, T., Seibert, J. J., Vu, L., Andres, R. J., Bolt, R. M., Bond, T. C., Dawidowski, L., Kholod, N., Kurokawa, J.-I., Li, M., Liu, L., Lu, Z., Moura, M. C. P., O'Rourke, P. R., and Zhang, Q.: Historical (1750–2014) anthropogenic emissions of reactive gases and aerosols from the Community Emissions Data System (CEDS), *Geosci. Model Dev.*, 11, 369–408, <https://doi.org/10.5194/gmd-11-369-2018>, 2018.

Hoesly, R., Smith, S., Ahsan, H., Prime, N., O'Rourke, P., Crippa, M., Klimont, Z., Guizzardi, D., Feng, L., Harkins, C., MCDONALD, B., & Wang, S.: CEDS v_2025_04_18 Gridded Emissions Data 0.5 degree (v_2025_03_18) [Data set]. Zenodo. <https://doi.org/10.5281/zenodo.15127477>, 2025.

Janssens-Maenhout, G., Crippa, M., Guizzardi, D., Dentener, F., Muntean, M., Pouliot, G., Keating, T., Zhang, Q., Kurokawa, J., Wankmüller, R., Denier van der Gon, H., Kuenen, J. J. P., Klimont, Z., Frost, G., Darras, S., Koffi, B., and Li, M.: HTAP_v2.2: a mosaic of regional and global emission grid maps for 2008 and 2010 to study hemispheric transport of air pollution, *Atmos. Chem. Phys.*, 15, 11411–11432, <https://doi.org/10.5194/acp-15-11411-2015>, 2015.

Lamarque, J.-F., Shindell, D. T., Josse, B., Young, P. J., Cionni, I., Eyring, V., Bergmann, D., Cameron-Smith, P., Collins, W. J., Doherty, R., Dalsoren, S., Faluvegi, G., Folberth, G., Ghan, S. J., Horowitz, L. W., Lee, Y. H., MacKenzie, I. A., Nagashima, T., Naik, V., Plummer, D., Righi, M., Rumbold, S. T., Schulz, M., Skeie, R. B., Stevenson, D. S., Strode, S., Sudo, K., Szopa, S., Voulgarakis, A., and Zeng, G.: The Atmospheric Chemistry and Climate Model Intercomparison Project (ACCMIP): overview and description of models, simulations and climate diagnostics, *Geosci. Model Dev.*, 6, 179–206, <https://doi.org/10.5194/gmd-6-179-2013>, 2013.

Randles, C. A., da Silva, A. M., Buchard, V., Colarco, P. R., Darmenov, A., Govindaraju, R., Smirnov, A., Holben, B., Ferrare, R., Hair, J., Shinozuka, Y., and Flynn, C. J.: The MERRA-2

Aerosol Reanalysis, 1980 Onward. Part I: System Description and Data Assimilation Evaluation, *J. Climate*, 30, 6823–6850, <https://doi.org/10.1175/JCLI-D-16-0609.1>, 2017.

Strode, S. A., Ziemke, J. R., Oman, L. D., Lamsal, L. N., Olsen, M. A., and Liu, J.: Global changes in the diurnal cycle of surface ozone, *Atmos. Environ.*, 199, 323–333, <https://doi.org/10.1016/j.atmosenv.2018.11.028>, 2019.

Todling, R. and El Akkraoui, A.: The GMAO Hybrid Ensemble-Variational Atmospheric Data Assimilation System: Version 2.0, <https://gmao.gsfc.nasa.gov/media/publications/zbly36ziNFDFbmYmvhQeVqPhUo/Todling1019.pdf>, 2018.